Journal of Technical Physics, J. Tech. Phys., **41**, 1, *Special Issue*, 183-202, 2000
Polish Academy of Sciences, Institute of Fundamental Technological Research, Warszawa
Military University of Technology, Warszawa

MODELING OF RADIO-FREQUENCY AND DIRECT CURRENT GLOW DISCHARGES IN ARGON

A. BOGAERTS and R. GIJBELS

DEPERTMENT OF CHEMISTRY, UNIVERSITY OF ANTWERP
Universiteitsplein 1, B-2610 Wilrijk-Antwerp, Belgium

A hybrid modeling network, consisting of Monte Carlo, fluid and collisional-radiative models for the various plasma species (electrons, argon ions, fast argon atoms, argon atoms in various excited levels, copper atoms and ions, also in various energy levels) has been developed for glow discharges, both in the direct current (dc) and the capacitively coupled radio-frequency (rf) mode at 13.56 MHz. The typical results, like electrical characteristics, densities of the various plasma species, collisions in the plasma, cathode-sputtering and optical emission intensities, are presented and compared between the two operation modes. It is found that for the same input power and pressure, the rf-mode requires lower voltages than the dc-mode, in good correlation with experiment. The cathode-sputtering (erosion) rate and the optical emission intensities are, however, calculated to be more or less similar for both discharge modes, which is also in agreement with experiment.

1. Introduction

Glow discharges are used in a large number of application fields, e.g., the semiconductor industry (for etching and deposition of layers), the materials technology (for deposition of protecting films), the laser-, lamp- and plasma display panel industry, and also in analytical chemistry, for the spectroscopic analysis of solid materials (e.g., [1, 2]). In the latter application field, direct current (dc) discharges are very often applied, due to their simplicity and ease of operation. The material to be analyzed is then used as the cathode of the glow discharge, which is being sputtered by the plasma species. The sputtered atoms can become ionized or excited in the plasma. The so-formed ions can be measured in a mass spectrometer whereas the excited sputtered atoms create characteristic photons, which can be detected with an optical emission spectrometer. However, the straightforward application of a dc glow discharge is limited to the analysis of conducting materials, because non-conducting cathode materials would be charged up due to positive ion bombardment, preventing the cathode from being sputtered any further. To widen the application field to the analysis of

non-conducting materials as well, interest is nowadays being shifted to radio-frequency discharges, mainly at 13.56 MHz (e.g., [3, 4]). Indeed, the material to be analyzed serves now as the rf-electrode of the discharge, and charge accumulation due to positive ion bombardment can be neutralized due to negative charge accumulation by electron bombardment during part of the rf-cycle.

For good analytical practice, a thorough understanding of the glow discharge processes is desirable. We try to obtain this by modeling. Of course these models are not only valid for analytical glow discharges, but they can also be applied to glow discharges used in other application fields. In previous years we have developed a comprehensive modeling network (consisting of Monte Carlo, fluid and collisional-radiative models) for the various species present in a dc glow discharge, i.e., electrons, argon ions, fast argon ground state atoms, argon atoms in various excited levels, sputtered copper atoms and the corresponding ions, also in the ground state and in various excited levels (e.g., [5, 6, 7, 8, 9, 10, 11]). More recently, we have developed a similar model, consisting of the same sub-models, for a 13.56 MHz rf discharge (see e.g., [12, 13, 14, 15]). In the present paper, a brief overview of the modeling network is given, and some typical results are presented and compared for the two operation modes. The typical conditions for spectrochemical glow discharges are: argon discharge gas at several Torr pressure, 500-1200 V discharge voltage, 1 - 100 mA current and 1 - 100 W electrical power. The discharge cells are typically a few cm^3 in volume.

2. Description of the models

In the literature, different modeling approaches are presented to describe glow discharges: analytical or global models (e.g., [16]), fluid approaches (e.g., [17]), collisional-radiative models (e.g., [18]), full solutions of the Boltzmann equation (e.g., [19]), Monte Carlo methods (e.g., [20]), particle-in-cell models (e.g., [21]) and hybrid combinations of the above mentioned models (e.g., [22]). All the above models have their particular advantages and disadvantages, i.e., some of the models give a quick prediction but are only crude approximations, whereas other models are more accurate but require a long calculation time. Therefore, we use a specific model depending on the type of plasma species to be described. Indeed, the "fast" plasma species, like fast electrons, which are not in equilibrium with the electric field (which means that the electrons gain more energy from the electric field than they lose locally by collisions), are treated with a Monte Carlo model, which is most accurate for such species. The "slow" plasma species, on the other hand, like slow electrons, atoms, ions in the bulk plasma, for which a Monte Carlo model would take a very long calculation time, are handled with a fluid model, because the "equilibrium-approach" is justified here. Furthermore, the atoms and ions in excited levels are described with a collisional-radiative model, which can be considered as a kind of fluid model. All the different models are then combined into a hybrid modeling network, to present an overall picture of the glow discharge. The different species assumed to be present in the plasma, and the models used to describe these species, are presented in Table 1. The Monte Carlo models are developed in three dimensions; the fluid and collisional-

radiative models are only in two dimensions, because the cell geometry to be simulated has a cylindrical symmetry, and hence the three dimensions could be reduced to two dimensions (axial and radial direction). In the following, each of these models will be briefly explained.

Table 1. Overview of the species assumed to be present in the plasma, and the models used to describe these species

Plasma species	Model
thermal Ar atoms	no model, assumed uniformly distributed
electrons	Monte Carlo model for fast electrons fluid model for slow electrons
Ar ions	fluid model (together with the slow electrons + coupled to Poisson equation) Monte Carlo model in sheath
fast Ar atoms (created from Ar ions by collisions)	Monte Carlo model in sheath
excited Ar atoms (65 levels)	collisional-radiative model
Cu atoms: thermalization process	Monte Carlo model
Cu atoms + ions: ground + excited levels	collisional-radiative model
Cu ions	Monte Carlo model in sheath

2.1. Monte Carlo model for the fast electrons

Electrons are emitted from the cathode or rf-electrode due to positive argon ion bombardment, and they are accelerated in the sheath due to the strong electric field. These electrons are followed with a Monte Carlo model, as well as the electrons created in the sheath by ionization collisions.

A large number of "super-electrons", corresponding to several "real" electrons, is followed, one after the other, as a function of time. During successive time-steps, their trajectory is calculated with Newton's laws, and their collisions are treated with random numbers. Indeed, the probability of collision during that time-step is calculated (yielding a value between 0 and 1) and compared to a randomly created number between 0 and 1. If the calculated probability is lower than the random number, no collision takes place. If the collision probability is higher than the random number, a collision event occurs. Collision processes taken into account in this model are elastic collisions with Ar atoms, electron impact ionization, excitation and de-excitation between the different Ar and Cu (excited) levels, and electron-electron Coulomb scattering. To determine which collision takes place, the partial collision probabilities of the various collision types are calculated, and the total collision probability (= the sum of the partial probabilities) is subdivided in intervals with lengths corresponding to these partial probabilities. Then, a second random number is generated and

the interval into which this random number falls, determines the type of collision that takes place. Further, the new energy and direction after collision are also determined by random numbers, based on energy conservation laws and on differential scattering cross sections. Then, the same procedure is repeated for the next electron during the same time-step, until all electrons are followed. Then, we proceed to the next time-step. This procedure is repeated during a large number of time-steps until (periodic) steady-state is reached. This happens already, in the rf-case at 13.56 MHz, after two rf-cycles (i.e., about $1.5 \cdot 10^7$ seconds). It should be mentioned that in the dc-case, the calculations can also be carried out independently of time.

In order to reduce the calculation time, only "fast" electrons are followed with this Monte Carlo model. When the electrons arrive in the bulk plasma and have energies lower than the threshold for inelastic collisions, they are "transferred to the slow electron group", to be followed with the fluid model (see below). More details of this Monte Carlo model can be found in Refs. [5, 6, 8, 12].

2.2. Fluid model for slow electrons, Ar ions and potential distribution

The slow electrons are followed with a fluid model, together with the Ar ions. The equations to be solved in this model are the first two (or three) moments of the Boltzmann transport equation, i.e., the mass continuity equations for slow electrons and Ar ions (Eqs. 2.1 and 2.2), and the momentum continuity equations for electrons and ions, which could be reduced to the transport equations, based on diffusion and drift in the electric field (Eqs. 2.3 and 2.4). Moreover, for the electrons also the electron energy balance equation is solved (Eq. 2.5). Finally, these equations are coupled to Poisson's equation, to obtain self-consistently the potential distribution from the electron and ion densities (Eq. 2.6):

$$\frac{\partial n_{Ar^+}(z,r,t)}{\partial t} + \overline{\nabla} \cdot \overline{j_{Ar^+}}(z,r,t) = R_{Ar^+}(z,r,t), \tag{2.1}$$

$$\frac{\partial n_e(z,r,t)}{\partial t} + \overline{\nabla} \cdot \overline{j_e}(z,r,t) = R_e(z,r,t), \tag{2.2}$$

$$\overline{j_{Ar^+}}(z,r,t) = \mu_{Ar^+} n_{Ar^+}(z,r,t) \overline{E}^{eff}(z,r,t) - D_{Ar^+} \overline{\nabla} n_{Ar^+}(z,r,t), \tag{2.3}$$

$$\overline{j_e}(z,r,t) = \mu_e n_e(z,r,t) \overline{E}(z,r,t) - D_e \overline{\nabla} n_e(z,r,t), \tag{2.4}$$

$$\frac{\partial w_e(z,r,t)}{\partial t} + \overline{\nabla} \cdot \left(-\frac{5}{3} \mu_e w_e(z,r,t) \overline{E}(z,r,t) - \frac{5}{3} D_e \overline{\nabla} w_e(z,r,t) \right) = -e\overline{j_e}(z,r,t) \cdot \overline{E}(z,r,t) - R_{w,e}(z,r,t), \tag{2.5}$$

$$\nabla^2 V(z,r,t) + \frac{e}{\varepsilon_0} \left(n_{Ar^+}(z,r,t) - n_e(z,r,t) \right) = 0, \overline{E} = -\overline{\nabla} V, \tag{2.6}$$

where n and j are the argon ion and electron densities and fluxes, R_{Ar^+} and R_e are the argon ion and electron creation rates, μ and D are the ion and electron mobility and diffusion coefficient, E and E^{eff} are the electric field and the effective electric field (as felt by the ions, see [12]), w_e is the electron energy density (i.e., ε_e times n_e), $R_{w,e}$ presents the energy loss by collisions, V is the electric potential, and e and ε_0 are the electron charge and vacuum permittivity, respectively.

These equations are strongly coupled and solving them is no straightforward mathematical problem. The method we used was developed by Goedheer and coworkers [23, 24] and is based on the Scharfetter-Gummel exponential scheme [25, 26].

Finally, it should be mentioned that the electrons in this fluid model, especially in the rf-case, can gain again some energy from the electric field, and they give rise to some more inelastic collision processes which should be taken into account in the model. In the rf-case, it was demonstrated that the ionization produced by these slow fluid-electrons which gain again sufficient energy from the oscillating electric field (i.e., so-called a-ionization) is clearly dominant compared to the ionization calculated in the Monte Carlo model [12]. Further details about this fluid model are found in Refs. [6, 8, 12].

2.3. Monte Carlo model for the Ar ions and fast Ar atoms

Because a fluid model is less suitable for species not in equilibrium with the electric field (which means that they gain more energy from the electric field than they lose by collisions), and since the Ar ions are not in equilibrium with the rather high electric field in the sheath region adjacent to the rf-electrode (cathode), these species are also described with a Monte Carlo model in this region. Furthermore, this model also treats the fast Ar atoms, which are created from the Ar ions in the sheath by charge transfer and momentum transfer scattering collisions. The principle is the same as for the electron Monte Carlo model. Collision processes incorporated in this Monte Carlo model are charge transfer collisions for the Ar ions, and momentum transfer collisions, ionization, excitation and de-excitation collisions for the different Ar and Cu excited levels, for both the Ar ions and fast Ar atoms. In this Monte Carlo model, the Ar ions and fast Ar atoms are also followed as a function of time, until periodic steady state is reached, which is the case after about 25 - 30 rf-cycles for these species. For more details, we refer to Refs. [7, 13].

2.4. Collisional-radiative model for the Ar excited levels

64 excited Ar levels are incorporated in this model. Some of them are individual levels (e.g., the 4s levels), but most of them are effective levels (i.e., a group of individual levels with similar excitation energy and quantum numbers). For each of these levels, a balance equation is solved, with different populating and depopulating processes. The processes taken into account include electron, Ar ion and atom impact ionization, excitation, de-excitation and three-body recombination for all levels, radiative recombination and radiative decay between all

levels, and Hornbeck-Molnar associative ionization for the levels with excitation energy above 14.71 eV. Moreover, for the Ar 4s levels some additional processes are incorporated, like Ar^*-Ar^* (associative) ionization, Penning ionization of sputtered Cu atoms, three-body collisions with Ar atoms, and radiation trapping for the resonant levels, which radiate to the Ar ground state. The radiation trapping is described by means of an escape factor, which represents the fraction of photons that can really escape from the plasma without being reabsorbed by the argon ground state atoms. Transport of the excited species (by diffusion) can be neglected with respect to the collision and radiation processes. The fact that all these processes are of collisional or radiative nature explains the name of this model. More information about this model can be found in Refs. [9, 14].

2.5. Monte Carlo model for the thermalization of the sputtered Cu atoms

When the Cu atoms are sputtered from the cathode (due to Ar ion, fast Ar atom and Cu ion bombardment), they have energies of 5 - 10 eV, which they lose almost immediately by collisions with the Ar gas atoms, until they are thermalized. Because this thermalization process occurs almost "immediately", it is finished before the Cu atoms start to move by diffusion. Because both processes are, hence, separated in time, their description can be subdivided in two separate models. The thermalization process is treated in a Monte Carlo model, similar to the electron Monte Carlo model (for more details of this thermalization model: see Ref. [10]). It results in a so-called thermalization profile (i.e., distribution of thermalized Cu atoms as a function of distance from the electrode), which serves as initial distribution for the diffusion of the thermalized Cu atoms, which is described in the next model.

2.6. Collisional-radiative model for the Cu atoms, Cu^+ and Cu^{++} ions in the ground state and in various excited levels

As mentioned above, the further transport of the sputtered Cu atoms after thermalization occurs by diffusion. Moreover, these Cu atoms can be ionized and/or excited. The behavior of the Cu atomic and ionic ground state and excited levels is described again in a collisional-radiative model. 8 Cu atomic levels, 7 Cu^+ ionic levels, as well as the Cu^{++} ions (no subdivision in different levels) are considered in this model; again most of the levels are effective levels, consisting of various individual levels. For each level, a balance equation is constructed with different populating and depopulating processes. The processes taken into account for each level are electron and atom impact ionization, excitation, de-excitation and radiative decay, as well as three-body recombination to the highest excited levels, Penning ionization by Ar metastable atoms and asymmetric charge transfer with Ar ions for some specific levels. Furthermore, transport occurs by diffusion for the Cu atoms and by diffusion and drift in the electric field for the Cu ions, but this is again negligible for the excited levels compared to the collision and radiation processes. More detailed information about this model can be found in Refs. [11, 15].

2.7. Monte Carlo model for the Cu ions in the sheath

Similar to the Ar ions, the Cu ions are not in equilibrium either with the high electric field in the sheath adjacent to the rf-electrode (cathode), and are therefore also described with a Monte Carlo model in this region. This model is very similar to the Ar ion and fast Ar atom Monte Carlo model. It should be mentioned that these two Monte Carlo models in the sheath region are especially important for calculating the Ar ion, fast Ar atom and Cu ion flux energy distributions bombarding the rf-electrode (cathode), which are needed to calculate the amount of sputtering.

2.8. Coupling of the models

All these models are coupled to each other due to the interaction processes between the different plasma species, and the output of one model serves as the input for the next model (e.g. creation rate of certain species due to collisions of other kinds of species). Therefore, all the models are solved iteratively until final convergence is reached. More information about this coupling, which is identical for the dc and rf mode, can be found, e.g., in Ref. [27]. The whole calculation procedure for one set of discharge parameters takes several days on a Digital personal workstation.

3. Results of the models

3.1. Electrical characteristics

There is essentially a difference between the type of input and output parameters in the dc and rf model. In the dc model, the voltage, gas pressure and temperature are used as input parameters, and the electrical current (and hence also the power) follow from the calculations. In the rf model, on the other hand, the electrical power is used as input parameter, beside the gas pressure and temperature, and the voltage (both rf amplitude and dc bias voltages) result as output values. However, the dc case can also be simulated with the rf model (when keeping the voltage at the cathode constant), and the results were totally identical to the dc model results.

In order to check the modeling calculations against experimental values, we have performed the calculations for typical cell dimensions used experimentally, although we have approximated the rather complicated experimental cell geometry by a simple cylinder, with length equal to 2 cm and diameter equal to 2.5 mm. The cathode or rf-electrode is placed at one end of the cylinder (hence also with diameter of 2.5 mm) and the other cell walls are grounded. Because of the large difference in size of rf-electrode and grounded electrode, it is expected that, in the rf-case, the dc-bias voltage is fairly negative. Indeed, typical experimental discharge conditions reveal, at a frequency of 13.56 MHz, a dc bias voltage of -627 V and an rf amplitude voltage of 764 V, for a gas pressure of about 6 Torr and electrical power of 10 W [28]. It is also observed experimentally that the dc operation mode yields similar analytical characteristics (sputter-erosion rates,

optical emission intensities) at the same power and pressure values, but that this occurs at the higher voltage of 1100 V [28].

Fig. 1 presents the calculated (solid line) and experimental (dashed line) potentials at the rf-electrode as a function of time in the rf-cycle. Both have a

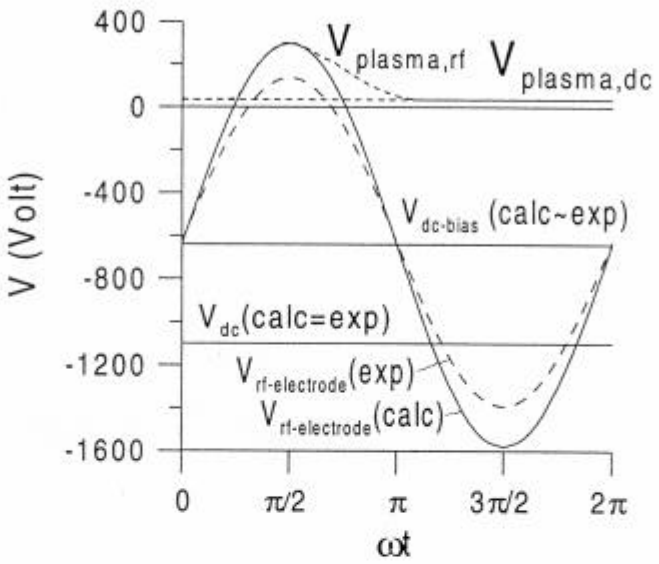

FIG. 1. Electrical potential at the rf-electrode ($V_{rf-electrode}$: calculeted (solid line) and experimental (dashed line)), dc-bias voltage ($V_{dc-bias}$) and plasma potential ($V_{plasma,rf}$ in the rf-discharge. Also shown are the voltage (V_{dc}) and plasma potential ($V_{plasma,dc}$) in the dc discharge. Operating conditions: $p = 6$ Torr, $P = 10$ W.

sinusoidal profile. Indeed, this is used as input in the model. Experimentally, however, the real profile differs slightly (less than 10% for the present case) from a perfect sinusoidal profile. The potential at the rf-electrode is negative during most of the rf-cycle, in both the real and the calculated conditions, and becomes only positive around $\pi/2$. The calculated rf-amplitude voltage is about 937 V, which is about 170 V higher than the experimental value (i.e., 764 V). The calculated dc-bias voltage of - 640 V is however in very good agreement with experiment (i.e., - 627 V). Also the calculated voltage in the dc case, for exactly the same conditions of power and pressure, is presented, and is equal to -1100 V. This value is also in very good agreement with the measured value. Although the absolute values of these calculation results, in particular the rf-amplitude, are not in exact agreement with the experimental values, the correct trend is certainly predicted. Indeed, the rf voltages (both rf-amplitude and dc-bias) are clearly lower than the dc voltage for the same conditions of pressure and power, which indicates that the rf mode yields more efficient ionization, due to the movement of electrons in the oscillating electric field (see further). The plasma potentials in the rf mode and dc mode are, however, very similar to each other, as is also illustrated in Fig. 1. The rf plasma potential is rather high (almost 300 V, i.e., equal to the potential at the rf-electrode) around $\pi/2$, but decreases to values of about 35 V during most of the rf-cycle, which is equal to the dc plasma potential.

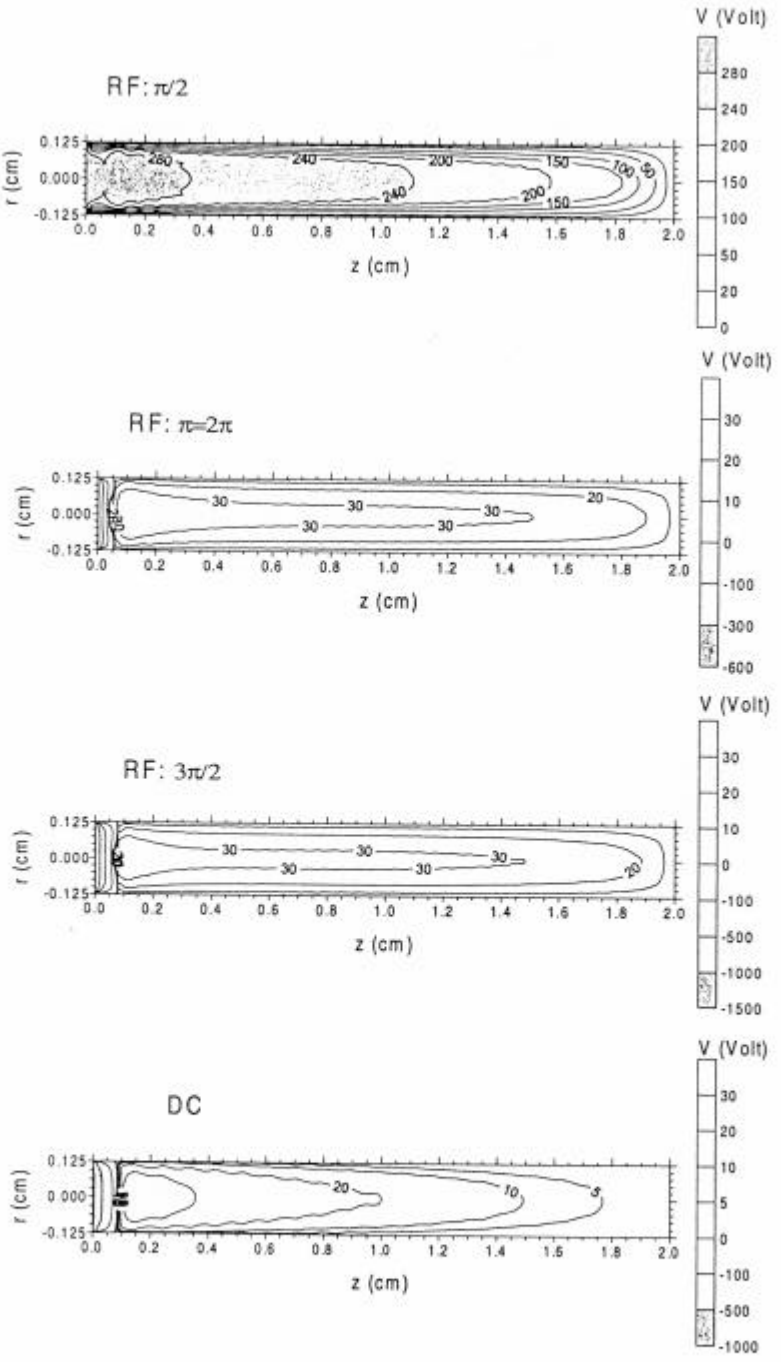

FIG. 2. Two-dimensional potential distributions in the rf-discharge, at 4 times in the rf-cycle, and in the dc-discharge. Same operating conditions as in Fig. 1.

The two-dimensional potential distributions, at four times in the rf-cycle in the rf-case, and the dc potential distribution, are presented in Fig. 2. At $\omega t = \pi/2$, the potential is rather high throughout the main discharge volume, but it decreases gradually, and close to the grounded walls more rapidly, to zero

at the grounded cell walls. Hence, at this time in the rf-cycle, there is no rf-sheath adjacent to the rf-electrode, but rather adjacent to the grounded cell walls. At $\omega t = 0$, π and 2π, the potential is very negative (i.e., -640 V, the dc-bias) at the rf-electrode and it increases rapidly to zero at 0.4 mm from the rf-electrode. It reaches a positive value of about 35 V in the bulk plasma. A similar potential distribution is also observed around $\omega t = 3\pi/2$, but the potential at the rf-electrode is even more negative (i.e., about -1580 V, equal to the sum of the rf-amplitude and dc-bias). This large potential has dropped to zero at about 0.6 mm from the rf-electrode, and the value in the bulk plasma is also about 35 V. The potential distributions at $\omega t = 0$, π or 2π and $\omega t = 3\pi/2$ strongly resemble the dc potential distribution, which is also shown in Fig. 2. It is -1100 V at the cathode, goes through zero at about 0.8 mm from the cathode, and reaches also a value of 35 V in the bulk plasma (negative glow). Hence, for the discharge conditions and cell geometry under study, it can be concluded that, except around $\omega t = \pi/2$, the rf potential distribution looks very much like a dc potential distribution due to the large dc-bias, so that the present rf discharge can be considered as a dc discharge with an rf sine-wave superimposed to it.

Not only the electrical potential follows from the calculations; also the electrical current. Fig. 3 depicts the total rf-current, as a function of time in the rf-cycle, as well as the individual contributions of electron current, ion current

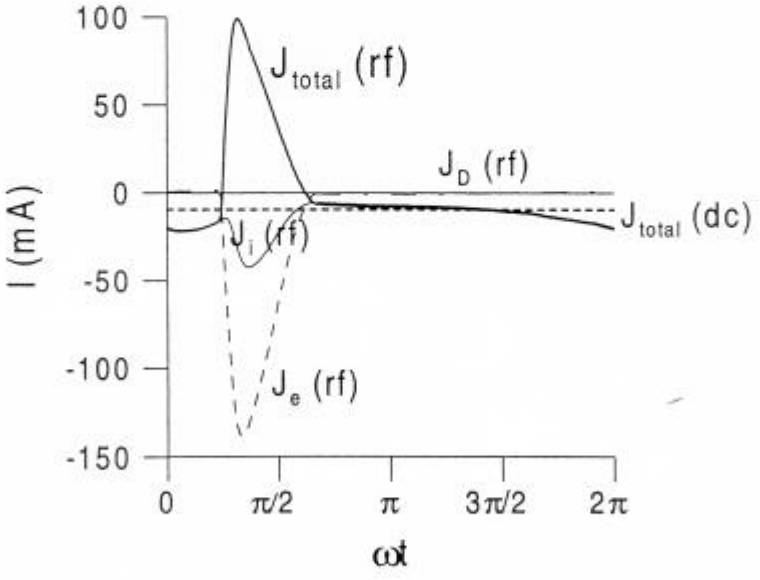

FIG. 3. Total electrical current at the rf-electrode ($J_{total}(rf)$) in the rf-discharge, and contributions of the ion current ($J_i(rf)$), electron current ($J_e(rf)$ and displacement current ($J_D(rf)$), also at the rf-electrode, as a function of time in the rf-cycle. Also shown is the total electrical current at the cathode in the dc-discharge ($J_{total}(dc)$). Same conditions as in Fig. 1.

and displacement current (i.e., due to the movement of the rf-sheath). As follows from Fig. 3, the latter contribution is negligible at our discharge conditions. Indeed, the rf-sheath varies only in thickness between 0 mm (around $\omega t = \pi/2$), 0.4 mm (around $\omega t = 0$, π and 2π) and 0.6 mm (around $\omega t = 3\pi/2$), as could be observed in Fig. 2. This is not a large variation, and the positive charge in the

rf-sheath does not change enough to yield a large displacement current. During most of the rf-cycle, the current at the rf-electrode is attributed to ions bombarding the rf-electrode. However, around $\omega t = \pi/2$, a large electron current is drawn towards the rf-electrode. This is necessary to compensate for the positive charge accumulation at the rf-electrode due to the capacitive coupling of the rf-power, and it results in a net zero current at the rf-electrode, when integrated over the entire rf-cycle. Also plotted in Fig. 3 is the calculated current in the dc case, for the same conditions of power and pressure. It is equal to (-) 9 mA, which is most of the time lower than the instantaneous values in the rf-case (which is of course logical, because the dc voltage is higher for the same power value as in the rf-case).

3.2. Densities of the plasma species

In Fig. 4 the calculated argon ion densities in the rf and dc discharge are illustrated. The argon ion density was found to be constant throughout the entire

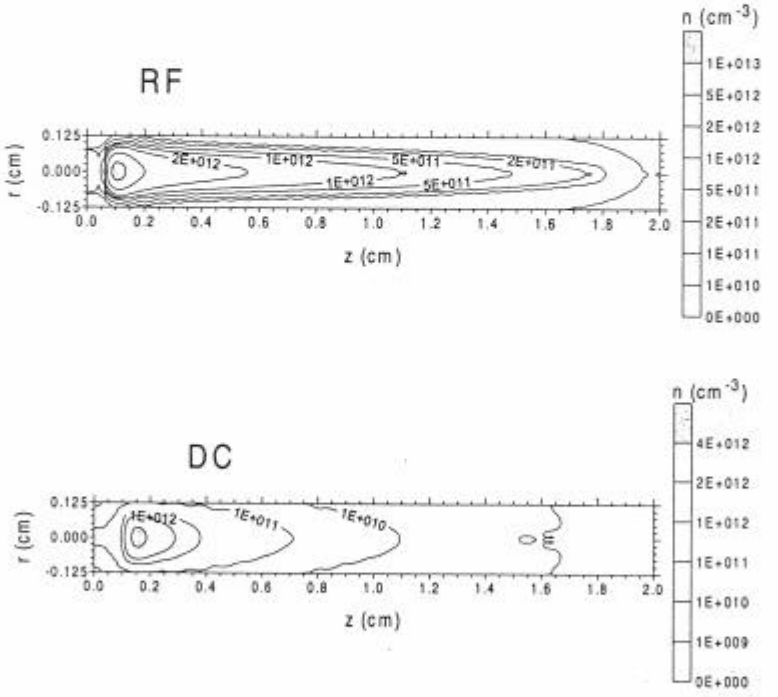

FIG. 4. Two-dimensional Ar ion density profile in the rf- and the dc-discharge. Same operating conditions as in Fig. 1.

rf-cycle. Qualitatively, the profiles look rather similar to each other, i.e. a low and nearly constant value in the sheath, a maximum between 0.1 and 0.2 mm from the electrode, and then decreasing to low values at the grounded cell walls. The rf density appears, however, to be a factor of 2.5 higher than the dc argon ion density, which is not unexpected, taking into account the somewhat higher rf-current and the more efficient rf ionization. Moreover, the rf argon ion density drops much slower to low values as a function of distance from the electrode than

the dc argon ion density. From this (and also from the electron and metastable argon atom density profiles; see below) it can be concluded that in the rf case, the discharge vessel is much more filled with plasma than in the dc case.

The electron density (not shown) is characterized by the same profile (also in absolute numbers) as the argon ion density, but it is zero in the sheath yielding a net positive space charge (and hence a strong potential drop; see above). Only around $\omega t = \pi/2$ in the rf-case, the electron and argon ion densities are equal to each other, yielding charge neutrality not only in the bulk plasma, but also in the sheath adjacent to the rf-electrode.

The calculated argon metastable densities ($4s[3/2]_2$ level) in both the rf and the dc case, are presented in Fig. 5.

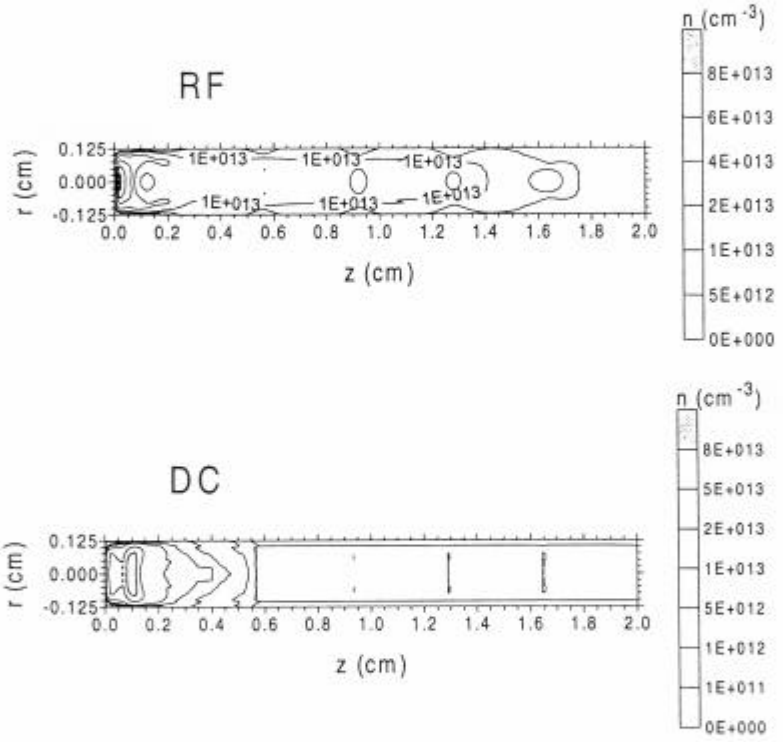

FIG. 5. Two-dimensional Ar metastable atom density profile ($4s[3/2]_2$ level) in the rf- and the dc-discharge. Same operating conditions as in Fig. 1.

Again, the metastable densities appear to be constant throughout the entire rf-cycle. Looking at the absolute values, the metastable densities are characterized by the same peak values in both the dc and rf discharge. The location of the peaks is, however, different. Indeed, the rf metastable density shows a pronounced peak adjacent to the rf-electrode and it has also rather high values throughout the entire bulk plasma. The latter is due to excitation by a-electrons around $\omega t = \pi/2$. Indeed, as has been demonstrated in ref. [12], electrons in the bulk plasma can become slightly heated by the moderate electric field in this region around $\omega t = \pi/2$ (see also Fig. 2), and they have just high enough energy to cause excitation and ionization (see also below). This excitation, which occurs primarily around $\omega t = \pi/2$, is responsible for the rather high values in

the bulk plasma. In the dc case, the metastable density shows a distinct peak at the interface between sheath and negative glow and is also quite high adjacent to the cathode. However, it is very low in the bulk plasma, due to the absence of a-electrons which can cause excitation here.

Fig. 6 presents the calculated sputtered copper atoms densities (in the ground state) in the rf (again constant in time) and dc discharge. The relative profiles

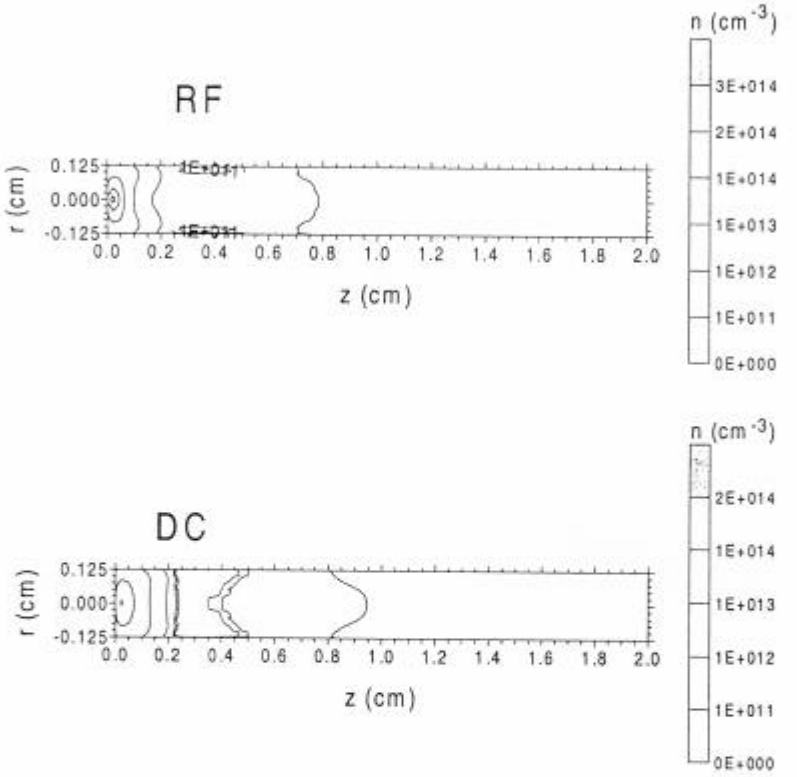

FIG. 6. Two-dimensional sputtered Cu atom density profile in the rf- and the dc-discharge. Same operating conditions as in Fig. 1.

are almost identical, i.e., low values at the electrodes and a maximum at less than 0.5 mm from the cathode (or rf-electrode). Also the absolute values are very similar. The value in the rf discharge is slightly higher (i.e., a factor of 1.5, only at the maximum of the profile), which is attributed to the somewhat more efficient sputtering (see below). The calculated copper ion densities (in the ground state) are also very similar to each other, both in relative profiles (i.e., maximum around 1 mm) and even in absolute values, as is demonstrated in Fig. 7. This finding is not straightforward, taking into account the clear differences in electric potentials, currents and argon ion and electron densities in both discharge modes (see above). It turns out that, although the model predicts slightly less efficient sputtering in the dc discharge, this appears to be compensated by slightly more efficient ionization. Finally, this good correlation between copper atom and ion densities in both discharge modes is in excellent agreement with experimental observations, where it is found that the rf and dc modes, at the same values of power and pressure but different values of voltage

(see above) yield very similar analytical characteristics (which are of course in close relation to the sputtered species) [28].

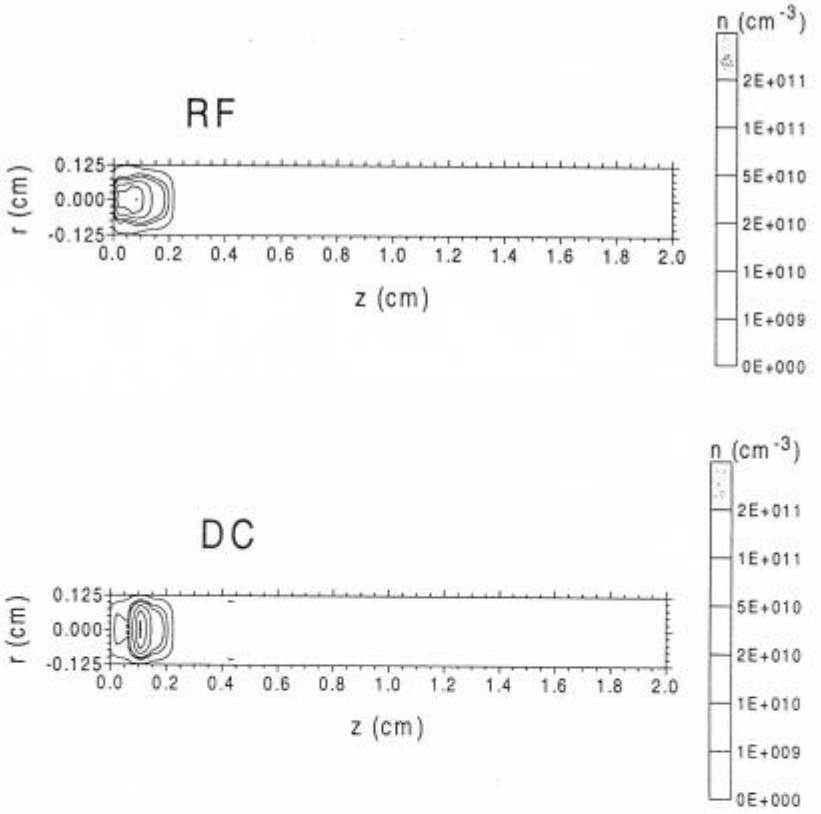

FIG. 7. Two-dimensional Cu in density profile in the rf- and the dc-discharge. Same operating conditions as in Fig. 1.

3.3. Ionization in the plasma

In Fig. 8 the electron impact ionization rate of argon in one dimension is plotted as a function of distance from the rf-electrode. In the rf model, the ionization due to electrons is described both in the Monte Carlo and the fluid model. Indeed, as mentioned before, the Monte Carlo model treats only the fast electrons, and once they are slowed down below the threshold for inelastic collisions in the bulk plasma, these electrons are transferred to the fluid model. However, these slow electrons can again be heated by the oscillating electric field (due to the movement of the rf-sheath) and by the moderate electric field in the bulk plasma around $\omega t = \pi/2$ (see above, Fig. 2). Hence, these electrons can produce some more ionization, which is typical for an rf-discharge and is called "α-ionization". The ionization rates due to Monte Carlo electrons (i.e., the electrons emitted by the rf-electrode and the fast electrons created in collisions from the first group; they produce so-called "γ-ionization") and due to fluid electrons, at four times in the rf-cycle, are presented in the top and middle parts of Fig. 8, respectively. The Monte Carlo (γ) ionization reaches a maximum at the sheath-bulk plasma interface. The fluid (α) ionization at times $\omega t = \pi$, $3\pi/2$ and 2π also reaches

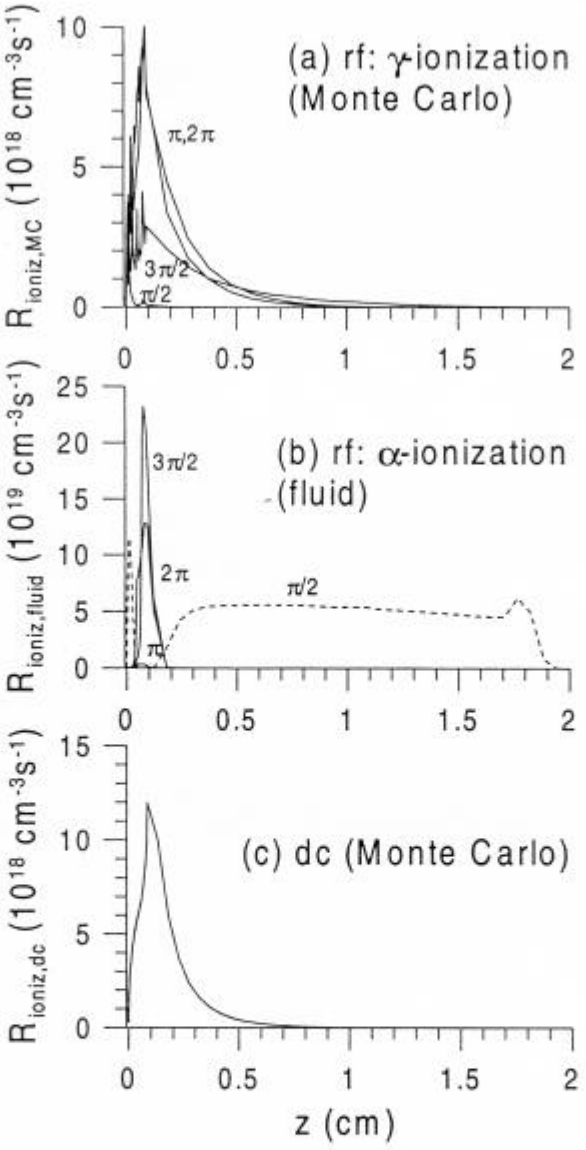

FIG. 8. Electron impact ionization rates as a function of distance from the rf-electrode/cathode, (a) in the rf-discharge at four times, calculated by the Monte Carlo model (γ- ionizatin), (b) in the rf-discharge at four times, calculated by the fluid model (α-ionization), (c) in the dc-discharge. Same operating conditions as in Fig. 1.

a maximum here, caused by electrons which are drawn towards the rf-electrode around $\omega t = \pi/2$ and then accelerated back towards the bulk plasma at later times, when the rf-sheath develops again and has a strongly negative electric field. The fluid ionization at $\omega t = \pi/2$ (presented by the dashed line in the middle part of the figure) is characterized by a peak adjacent to the rf-electrode (caused by the electrons drawn towards the rf-electrode) and a broad maximum in the entire bulk plasma (caused by electrons accelerated here by the moderate electric field). The latter broad maximum is also in correspondence with the

rather high values of the argon metastable density in the bulk plasma, as has been explained before. The lower part of Fig. 8 presents the electron impact ionization rate in the dc case. It reaches also a maximum at the sheath-negative glow interface, similar to the γ-ionization in the rf case, and is somewhat higher in magnitude than the time-averaged γ-ionization. However, in the dc case no α-ionization takes place, so that the overall dc ionization is lower than the overall rf ionization, yielding a higher dc voltage for the same conditions of power and pressure, in agreement with experiment.

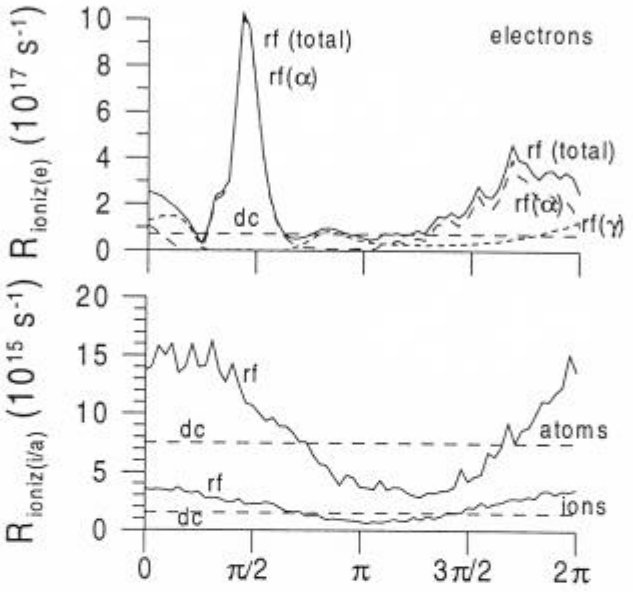

FIG. 9. Ionization of argon integrated over the entire discharge volume, in the rf-discharge (as a function of time in the rf-cycle) and the dc-discharge. Upper part: electron impact ionization (and individual contributions α and γ ionization), lower part: fast Ar ion and atom impact ionization. Same operating conditions as in Fig. 1.

This is also illustrated in Fig. 9, which presents the ionization rate, integrated over the entire discharge volume, as a function of time in the rf-cycle. It is clear (upper part of the figure) that most of the rf ionization is due to fluid electrons (a-ionization). The latter is especially important around $\omega t = \pi/2$, as was expected already from the broad maximum in Fig. 8. Also shown for comparison is the dc ionization rate, integrated over the entire discharge volume. It is somewhat higher than the g-ionization, but clearly lower than the a-ionization, as was illustrated already in Fig. 8. The lower part of Fig. 9 shows the ionization rate due to fast Ar ions and atoms, both in the rf mode and the dc mode. It appears that these processes occur at a similar rate in both operation modes, when averaged over time. The cross sections of Ar ion and atom impact ionization start to rise only for energies above several 100 eV. Since the Ar ions and atoms can only reach high energies adjacent to the rf-electrode/cathode (where they have gained energy from the high electric field in the sheath), these processes only occur in this region. Integrated over the entire discharge region they are, therefore, of minor importance compared to electron impact ionization (see the left axis of upper and lower part of Fig. 9). We calculated relative contributions

for electron, Ar ion and Ar atom impact ionization of about 95%, 1% and 4%, respectively, in the rf-case, and about 89%, 2% and 9%, respectively, in the dc-case [29]. The reason that electron impact ionization is even more important in the rf-case is of course due to the dominant role of α-ionization.

3.4. Optical emission intensities

As mentioned in the introduction, dc and rf glow discharges are used in analytical chemistry, often in combination with optical emission spectrometers, to measure emission intensities. The collisional-radiative models for Ar and Cu, which we have briefly described above, allow to calculate the populations of various excited levels. When multiplying the latter with the Einstein transition probabilities for radiative decay, the optical emission intensities can be obtained, which are of interest for glow discharge optical emission spectrometry. Fig. 10 presents, as an example, the calculated Ar atomic spectra, both in the rf and dc mode. The

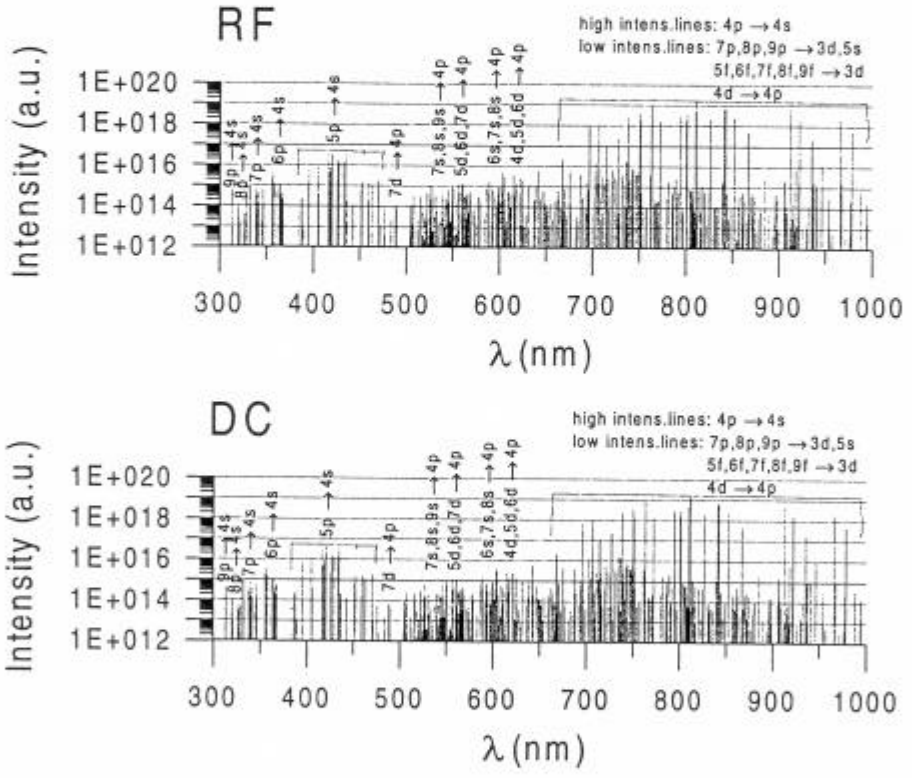

FIG. 10. Ar atomic optical emission spectra in the rf-and dc-discharge. Same operating conditions as in Fig. 1.

rf-spectrum is presented at $\omega t = 3\pi/2$; it varies only slightly as a function of time. It is clear that both spectra are almost identical, in spite of the different conditions of voltage and current (and electron and argon ion density). This is in excellent agreement with experiment, where it is also found that the rf and dc discharge, at the same conditions of power and pressure, but different values of voltage, yield very similar optical emission intensities. From both spectra it is obvious that the lines in the region 700-1000 nm, i.e., the so-called red

lines, corresponding to 4p-4s transitions, are the most intense ones. However, beside that, also the lines in the region 400-450, i.e., the so-called blue lines, corresponding to 5p-4s transitions, have rather high intensities, and there are many more lines, of lower intensity, throughout the whole spectrum studied. It was demonstrated before that the calculated spectrum, at least for the dc case where we have checked it, agreed very well with experimental spectra from the literature [30].

3.5. Sputtering at the cathode

Finally, the model is also able to calculate the amount of sputtering at the rf-electrode/cathode, based on the flux energy distributions of the Ar ions, fast Ar atoms and Cu ions calculated with the Monte Carlo models, and on an empirical formula for the sputtering yield as a function of the bombarding energy. Fig. 11 illustrates the net sputtering flux in the rf mode (as a function of time in the rf-cycle) and in the dc mode. The net sputtering flux is the result of the

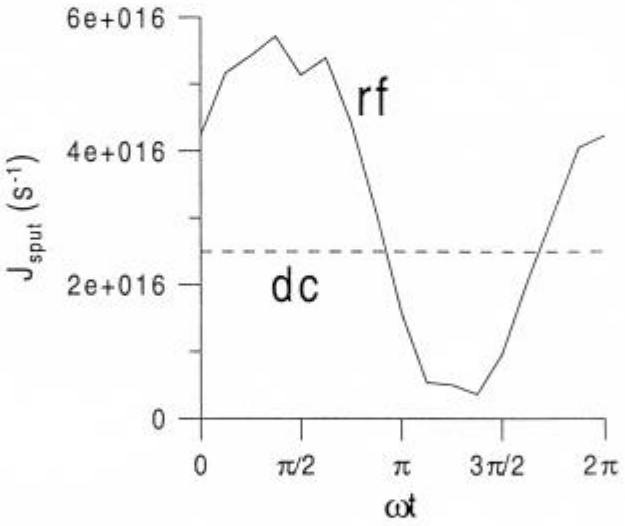

FIG. 11. Sputtering rate at the rf-electrode/cathode in the rf-and dc-discharge. Same conditions as in Fig. 1.

total sputtering flux, calculated in the way mentioned above, minus the flux of redeposited Cu atoms onto the electrode. The latter can be quite high, so that the net sputtering flux is only about 30-40% of the total sputtering flux. It can be deduced from Fig. 11 that, averaged over time, the rf sputtering flux is only slightly higher than the dc sputtering flux. This is not too much in discrepancy with experiment, where similar sputtering (erosion) rates are obtained in both the dc and rf mode, at the same values of power and pressure. Indeed, on one hand, the dc discharge is characterized by a higher voltage, yielding somewhat higher ion and atom energies at the cathode, which give rise to more efficient sputtering, but on the other hand, the rf discharge yields higher ion currents bombarding the rf-electrode, which leads of course also to more sputtering. It appears therefore that the combination of both effects yields more or less similar

sputtering in both operation modes.

Finally, it should be mentioned that the fast Ar atoms play a dominant role in sputtering, with a calculated contribution of about 70% in the rf-case and 60% in the dc-case. The Ar ions and Cu ions seem to contribute for about the same extent to the sputtering at the discharge conditions under study, i.e., Ar ions: about 17% (rf) and 21% (dc) and Cu ions (called "self-sputtering"): about 13% and 19% in the rf and dc case, respectively. The fact that the sputtering is predominantly caused by fast Ar atoms explains also why the rf case predicts more efficient sputtering around $\omega t = \pi/2$ and lowest sputtering around $\omega t = 3\pi/2$. Indeed, it was found in Ref. [13] that the fast Ar atoms have their maximum energy and maximum flux at the rf-electrode around $\omega t = \pi/2$, and that their energy and flux reach a minimum value around $\omega t = 3\pi/2$ [13].

4. Conclusion

A hybrid set of models (Monte Carlo, fluid and collisional-radiative models) has been developed for an argon glow discharge, both in the dc and the capacitively coupled rf mode. The species described with these models are the electrons, Ar ions, fast Ar atoms, Ar atoms in various excited levels, sputtered Cu atoms and the corresponding Cu ions, also in the ground state and in various excited levels. Some typical results, like electrical characteristics (voltages and currents), densities, ionization rates, optical emission spectra and information about sputtering, are presented here, as an example of what can be predicted with the models. It is found that the rf discharge requires lower voltages (both rf-amplitude and dc-bias) than the dc discharge, due to the more efficient ionization (i.e., so-called a-ionization). The calculated voltages are in reasonable agreement with experimental values, for the same conditions of power and pressure. On the other hand, the rf discharge is characterized by somewhat higher electrical currents (which is of course logical, in order to yield the same power values) and higher Ar ion and electron densities. Moreover, the argon ion, electron and argon metastable atoms have higher densities throughout the whole discharge in the rf case, whereas their densities drop rather quickly in the dc case. Hence, it can be concluded that the discharge vessel is much more filled with plasma in the rf case than in the dc case. The Cu atom and ion densities are, however, calculated to be more or less similar in both operation modes. This is also true for the optical emission spectra and the sputtering rates at the rf-electrode/cathode. The latter is also in good agreement with experiments. Beside the absolute values, the relative shapes of the profiles are also quite similar for both modes, except from a faster drop in the dc case. It can thus be concluded that, for the discharge conditions under investigation (i.e., rather high pressure, power and dc-bias, and small cell geometry), the rf discharge looks very much like a dc discharge.

Acknowledgments

A. Bogaerts is indebted to the Fund for Scientific Research (FWO-Flanders) for financial support. The authors also acknowledge financial support from the

Federal Services for Scientific, Technical and Cultural Affairs (DWTC/SSTC) of the Prime Minister's Office through IUAP-IV (Conv. $P4/10$). Finally, we wish to thank W. Goedheer, J. Vlcek and R. Carman for their valuable contributions to our models.

References

1. R.K. M.ARCUS, *Glow Discharge Spectroscopies*, Plenum Press, New York, 1993.
2. R. PAYLING, D.G. JONES, A. BENGTSON, *Glow Discharge Optical Emission Spectrometry*, Wiley, Chichester, 1997.
3. D.C. DUCKWORTH and R.K. MARCUS, Anal. Chem.,**61**, 1879, 1989.
4. V. HOFFMANN, H.-J. UHLEMANN, F. PRASSLER, K. WETZIG, D. BIRUS, Fresenius' J. Anal. Chem., 355, 826, 1996.
5. A. BOGAERTS, M. van STRAATEN, R. GIJBELS, Spectrochim. Acta Part B, **50B**, 179, 1995.
6. A. BOGAERTS, R. GIJBELS, W.J. GOEDHEER, J. Appl. Phys., **78**, 2233, 1995.
7. A. BOGAERTS, R. GIJBELS, J. Appl. Phys., **78**, 6427, 1995.
8. A. BOGAERTS, R. GIJBELS, W.J. GOEDHEER, Anal. Chem., **68**, 2296, 1996.
9. A. BOGAERTS, R. GIJBELS, J. VLCEK, J. Appl. Phys., **84**, 121, 1998.
10. A. BOGAERTS, M. van STRAATEN, R. GIJBELS, J. Appl. Phys., **77**, 1868, 1995.
11. A. BOGAERTS, R. GIJBELS, R.J. CARMAN, Spectrochim. Acta Part B, **53B**, 1679, 1998.
12. A. BOGAERTS, M. YAN, R. GIJBELS, W.J. GOEDHEER, J. Appl. Phys., **86**, 2990, 1999.
13. A. BOGAERTS, R. GIJBELS, IEEE Trans. Plasma Sci., in press.
14. A. BOGAERTS and R. GIJBELS, Spectrochim. Acta B, in press.
15. A. BOGAERTS and R. GIJBELS, Spectrochim. Acta B, in press.
16. S.V. BEREZHNOI, I.D. KAGANOVICH, L.D. TSENDIN, V.A. SCHWEIGERT, Appl. Phys. Lett., **69**, 2341, 1996.
17. J.-P. BOEUF, Phys. Rev. A, **36**, 2782, 1987.
18. J. VLCEK, J. Phys. D: Appl. Phys., **22**, 623, 1989.
19. J. BRETAGNE, G. DELOUYA, J. GODART, V. PUECH, J. Phys. D: Appl. Phys., **14**, 1225, 1981.
20. Z. DONKO, K. ROZSA, R.C. TOBIN, J. Phys. D: Appl. Phys., **29**, 105, 1996.
21. M. SURENDRA and D.B. GRAVES, IEEE Trans. Plasma Sci., **19**, 144, 1991.
22. Z. DONKO, Phys. Rev. E, **57**, 7126, 1998.
23. J.D.P. PASSCHIER, W.J. GOEDHEER, J. Appl. Phys., **73**, 1073, 1993.
24. J.D.P. PASSCHIER, W.J. GOEDHEER, J. Appl. Phys., **74**, 3744, 1993.
25. H.K. GUMMEL, IEEE Trans. Electron. Devices, **11**, 455, 1964.
26. D.L. SCHARFETTER, H.K. GUMMEL, IEEE Trans. Electron. Devices, **16**, 64, 1969.
27. A. BOGAERTS, R. GIJBELS, Plasma Phys. Reports, **24**, 573, 1998.
28. V. HOFFMANN, private communication.
29. A. BOGAERTS, R. GIJBELS, Spectrochim. Acta Part B, in press.
30. A. BOGAERTS, R. GIJBELS, J. VLCEK, Spectrochim. Acta Part B, **53**, 1517, (1998).